RSC Advances

PAPER

View Article Online
View Journal | View Issue

Check for updates

Cite this: *RSC Adv.*, 2018, **8**, 15773

$LiMg_{0.1}Co_{0.9}BO_3$ as a positive electrode material for Li-ion batteries†

Ceren Zor,[a] Mehmet Somer[a] and Semih Afyon*[b]

$LiCoBO_3$ could be a promising cathode material given the electronic and ionic conductivity problems are addressed. Here, Mg substitution in $LiCoBO_3$ is employed to stabilise the structure and improve the electrochemical performance. $LiMg_{0.1}Co_{0.9}BO_3$ is synthesised for the first time *via* sol–gel method and Mg substitution in the structure is verified by X-ray powder diffraction and energy dispersive X-ray analyses. The electrochemical properties are investigated by galvanostatic cycling and cyclic voltammetry tests. The composite electrode with conductive carbon (reduced graphite oxide and carbon black) delivers a first discharge capacity of 32 mA h g^{-1} within a 4.7–1.7 voltage window at a rate of 10 mA g^{-1}. The cycling is relatively stable compared to the unsubstituted $LiCoBO_3$. Mg substitution may enhance the electrochemical performance of borate-based electrode materials when combined with suitable electrode design techniques.

Received 29th March 2018
Accepted 17th April 2018

DOI: 10.1039/c8ra02745e

rsc.li/rsc-advances

Open Access Article. Published on 26 April 2018. Downloaded on 11/14/2018 9:13:47 AM.
This article is licensed under a Creative Commons Attribution-NonCommercial 3.0 Unported Licence.

1. Introduction

Li-ion batteries have been widely investigated and commercially used in many electronic applications including everyday portable devices since their commercialisation by Sony in 1990.[1] These batteries need to be developed further to meet the requirements of new portable devices, all-electric vehicles, stationary electric energy storage in a grid[2] and to be implemented in energy harvesting *via* wind, solar, and thermal sources.[3] Rechargeable Li-ion batteries with non-aqueous electrolytes enable higher operating voltages compared to conventional lead-acid and nickel-based batteries and are also suitable for novel electrode designs. One of the main drawbacks of Li-ion batteries is cathode materials with limited energy densities. Various cathodes including conversion type materials, organic molecules mimicking bioenergetics,[4] intercalation compounds of transition metal oxides, metal chalcogenides, and polyanion-based materials have been investigated to solve this problem and improve energy densities.

Currently, $LiFePO_4$, an olivine type polyanion cathode material, which is safer and cheaper than $LiCoO_2$ is also used as a popular cathode material in commercial applications.[5] Several other olivine type materials including $LiNiPO_4$,[6] $LiCoPO_4$,[6] and $LiMnPO_4$,[7] have been investigated as potential cathode materials as well. Moreover, other polyanions such as $(SO_4)^{2-}$,[8] $(BO_3)^{3-}$,[9] and $(SiO_4)^{4-}$[10] can be used in cathodes as promising frameworks with suitable transition metal cations. On a more practical note, due to their better stability regarding oxygen loss, polyanion cathode batteries could be safer than layered oxide cathode materials.[11] $(BO_3)^{3-}$-based cathode materials function similar to $(PO_4)^{3-}$-based ones and can be better alternatives owing to their lower weight and thus higher specific capacities. $(BO_3)^{3-}$-based cathode materials also offer the highest theoretical specific capacity among one-electron per formula unit polyanion systems[11] and they have not been extensively studied. First electrochemical investigation on borate-based Li-ion cathode materials was conducted by Legagneur *et al.*[9] on $LiFeBO_3$, $LiMnBO_3$, and $LiCoBO_3$ and they found that only 4%, 2%, and 1.5% Li per formula unit were extracted, respectively. The main reason hindering the practical specific capacities of $(BO_3)^{3-}$-based and other polyanion-based cathode materials is their limited ionic and electronic conductivities. Conductive coatings,[12,13] utilising interconnected nano-sized particles[14] or attaching the active material particles to conductive polymers[15] help overcoming the low electronic conductivity of these materials. One of the main strategies to improve electrochemical performance of poorly conducting electrode materials is decreasing the particle size to shorten the distance for Li^+ to travel upon charging/discharging.[12,16–18] Further investigations employing these strategies show that specific capacities over 100 mA h g^{-1} could be achieved for $LiMnBO_3$ which has a theoretical capacity of 222 mA h g^{-1},[16,19,20] and a capacity of 190 mA h g^{-1} could be achieved for $LiFeBO_3$ which has a theoretical capacity of 220 mA h g^{-1}.[21]

$LiCoBO_3$ is another interesting borate-based cathode candidate for rechargeable Li-ion batteries with a theoretical capacity of ~215 mA h g^{-1} and with a high potential for redox couple Co^{2+}/Co^{3+} operating at potentials above ~4.0 V *vs.* Li/Li^+.[22–24]

[a]Koc University, Department of Chemistry, 34450 Sariyer, Istanbul, Turkey. E-mail: msomer@ku.edu.tr; cezor@ku.edu.tr

[b]ETH Zurich, Department of Materials, CH-8093 Zurich, Switzerland. E-mail: semih.afyon@alumni.ethz.ch

† Electronic supplementary information (ESI) available. See DOI: 10.1039/c8ra02745e

Open Access Article. Published on 26 April 2018. Downloaded on 11/14/2018 9:13:47 AM.
This article is licensed under a Creative Commons Attribution-NonCommercial 3.0 Unported Licence.



However, at the current state of the art, the theoretical promise of this cathode material has not been achieved practically. The aforementioned strategies for polyanion-based cathodes such as the use of nano-sized particles, conductive coatings, composites, and several synthesis methods including solid-state,[9] sol–gel,[23,25] molten salt,[24] hydrothermal,[26] and polyacrylamide-gel methods[26] were also employed to improve the electrochemical properties $LiCoBO_3$. Afyon *et al.*[23] showed that reduced graphite oxide/nano-$LiCoBO_3$ composite delivers a first charge capacity of 55 mA h g^{-1} at C/20 rate, and by decreasing the particle size further Ragupathi *et al.*[25] claimed to obtain higher capacities. $LiCoBO_3$ was also prepared as a thin film *via* reactive magnetron sputtering and its electrochemical properties were investigated, where Khalifah and co-workers recorded no significant electrochemical response and reported a very low conductivity ($\sim 10^{-12}$ S cm^{-1}) value for $LiCoBO_3$.[27] The substitution of Co in $LiFeBO_3$ and $LiMnBO_3$ were also reported with $Li(Mn_{1-x}Co_x)BO_3$ (ref. 28) and $LiFe_{0.5}Co_{0.5}BO_3$ (ref. 29) delivering a capacity of 60 mA h g^{-1} at 1.8–4.7 V window and a capacity of 120 mA h g^{-1} at 1.5–4.7 V window, respectively.

Another strategy to improve the electrochemical properties of poorly performing polyanion-based cathode materials is doping of metal atoms at the transition metal site. The effect of Mg substitution in such cathode materials has been studied in various investigations.[11,30–33] Delmas *et al.*[34] showed that Mg doping increases the electronic conductivity and practical capacity in $LiMg_xCo_yO_2$ by creating defects in the structure. In another report, Mg was shown to decrease the charge transfer resistance in Li_2FeSiO_4/C.[31] Specifically for borate-based cathodes, Ceder and co-workers suggested Mg substitution in $LiMnBO_3$.[30] $LiMgBO_3$ has the similar monoclinic structure with $LiMnBO_3$ and Mg could be a candidate for structure stabilisation in $LiMBO_3$ materials.[30] They reported that phase decomposition of $LiMnBO_3$ decreases upon Mg substitution and the capacity retention over multiple cycles is improved. This effect was further investigated in a system where the material was partially substituted by Fe as well.[11] 98% of the theoretical capacity was achieved for $LiMn_{0.5}Fe_{0.4}Mg_{0.1}BO_3$ and the stability of the phase below 1.8 V upon discharge was enhanced by the prevention of conversion type reactions for $LiMBO_3$ (M = Fe and Mn).[11] The Li^+ ion transport mechanism in Fe and Mg substituted borate was also suggested to be different from the unsubstituted $LiMnBO_3$ resulting improved electrochemical properties.

In line with these earlier reports for various cathode materials, we adapt the Mg substitution in $LiCoBO_3$ and report on $LiMg_{0.1}Co_{0.9}BO_3$ here for the first time. The sol–gel synthesised $LiMg_{0.1}Co_{0.9}BO_3$ is electrochemically active delivering a first discharge capacity of 32 mA h g^{-1} at a rate of 10 mA g^{-1} within 4.7–1.7 V, and largely maintains this capacity over multiple cycles.

2. Experimental section

2.1. Synthesis

The gel-powder precursors were obtained *via* sol–gel method by dissolving stoichiometric amounts of $LiNO_3$, $Mg(NO_3)_2 \cdot 6H_2O$, $Co(NO_3)_2 \cdot 6H_2O$, and $B(OMe)_3$ in propionic acid. 0.01 mol $LiNO_3$ (≥99%, Alfa Aesar), 0.01 mol $Mg(NO_3)_2 \cdot 6H_2O$ (≥99%, Merck) and 0.01 mol $Co(NO_3)_2 \cdot 6H_2O$ (≥99%, Merck) were dissolved in 12 ml propionic acid (≥99%, Merck) at 80 °C for 3 h. Similarly, 0.01 mol $B(OMe)_3$ (≥99%, Merck) was added to 30 ml propionic acid and 50 ml ethanol (≥99.9%, Merck) mixture and heated following the same procedure. These two solutions were mixed together and heated at 80 °C for 1 h. 1 ml of distilled water was added to the final solution for hydrolysis and the heating continued until the evaporation was complete. The resulting gel-powder was annealed at ~750 °C for 10–15 h under ambient conditions for the preparation of $LiMg_{0.1}Co_{0.9}BO_3$. $LiCoBO_3$ was also synthesised following the same sol–gel protocol to compare the electrochemical performances.

2.2. Characterisation

The phase and the structure of the samples were determined by X-ray powder diffraction (XRD) method using a Bruker D8 Advance X-ray diffractometer and $CuK_{\alpha 1}$ radiation (operated at 40 mA, 40 kV). The homogeneous distribution of the Mg content was confirmed by energy-dispersive X-ray spectroscopy (EDX) performed with Zeiss Ultra Plus field emission GeminiSEM equipped with 123 eV resolution Bruker XFlash® 5010 EDS detector under 15 kV EHT. The particle size and the morphology of the samples were investigated by scanning electron microscopy (SEM) using the same field emission scanning electron microscope.

2.3. Electrochemical tests

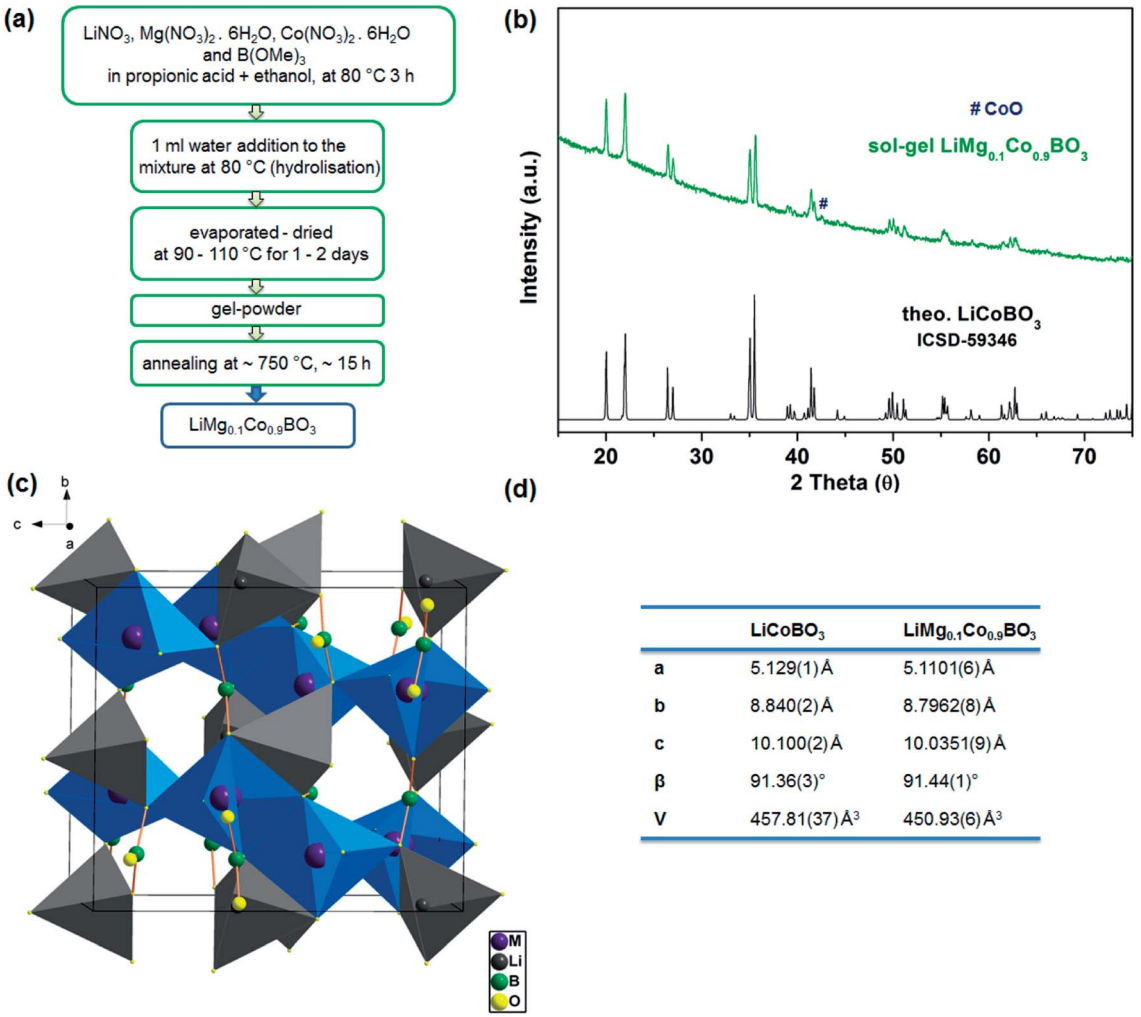
For the preparation of the cathode material, initially, 70 wt% active material $LiMg_{0.1}Co_{0.9}BO_3$ (or $LiCoBO_3$), 10 wt% conductive carbon (Super P), 10 wt% reduced graphite oxide (rGO), and 10 wt% PVDF (Sigma-Aldrich) were ground in an agate mortar. Then, a slurry of this powder was ultrasonically dispersed in toluene (≥99.9%, Merck) : THF (≥99%, Merck) (1 : 4) solution. For the fabrication of cathodes, this slurry was cast on Ti current collectors and dried at 80 °C for 3 h. The weight of active material on Ti current collectors was ~2 mg cm^{-2} after drying. For the fabrication of anodes, Li metal disks cut from Li rods were used. 1 M $Li[(C_2F_5)_3PF_3]$ in EC : DMC (1 : 1) (Merck, LF-30 SelectiLyte™) solution was used as the electrolyte in galvanostatic and cyclic voltammetry tests. Swagelok type of cells were put together in a glove-box under argon atmosphere using the described cathode, anode, and electrolyte, and glass and polypropylene/polyethylene/polypropylene separators. The galvanostatic cycling and cyclic voltammetry tests were carried out using a Metrohm Autolab PGSTAT30 potentiostat/galvanostat.

3. Results and discussion

The active material, $LiMg_{0.1}Co_{0.9}BO_3$, was synthesised through a sol–gel method. The gel-powder obtained from the stable sols of the homogenous mixture of nitrate salt precursors was annealed to reach the desired phase, as depicted in Fig. 1a. The X-ray powder diffraction (XRD) pattern of $LiMg_{0.1}Co_{0.9}BO_3$ is displayed in Fig. 1b. The reflections in the pattern can be

 This journal is © The Royal Society of Chemistry 2018

Open Access Article. Published on 26 April 2018. Downloaded on 11/14/2018 9:13:47 AM.
This article is licensed under a Creative Commons Attribution-NonCommercial 3.0 Unported Licence.



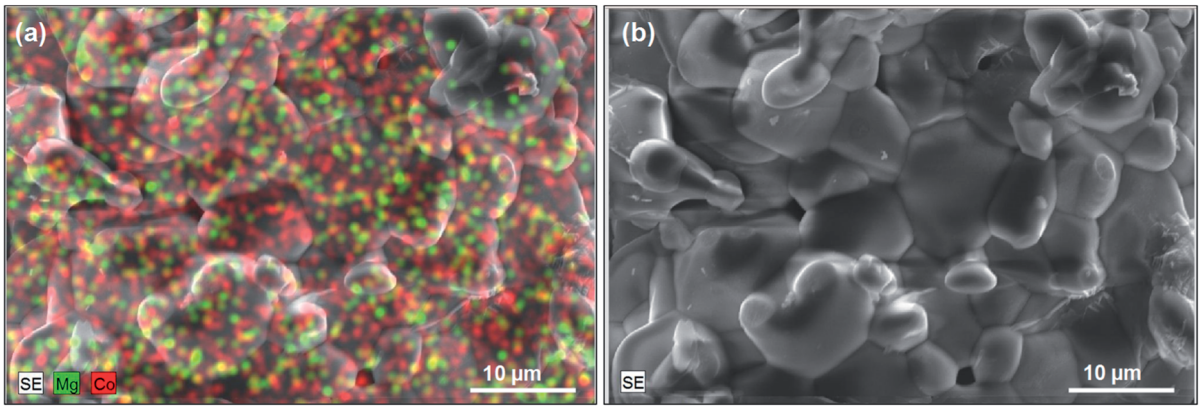
	$LiCoBO_3$	$LiMg_{0.1}Co_{0.9}BO_3$
a	5.129(1) Å	5.1101(6) Å
b	8.840(2) Å	8.7962(8) Å
c	10.100(2) Å	10.0351(9) Å
β	91.36(3)°	91.44(1)°
V	457.81(37) Å^3	450.93(6) Å^3

Fig. 1 (a) The synthesis scheme for $LiMg_{0.1}Co_{0.9}BO_3$, (b) XRD powder patterns of sol–gel synthesised novel $LiMg_{0.1}Co_{0.9}BO_3$ (green) (# represents CoO impurity) and calculated (ICSD 59346) $LiCoBO_3$ (black),[35] (c) crystal structure of $LiMg_{0.1}Co_{0.9}BO_3$ (skew [100] view of the phase, M = Co or Mg), and (d) lattice parameters for $LiCoBO_3$ (ref. 35) and $LiMg_{0.1}Co_{0.9}BO_3$.

matched to the calculated pattern for $LiCoBO_3$ (ICSD 59346)[35] and no major residual diffraction peaks are observed confirming the phase purity of the sample (Fig. 1b). However, a residual impurity peak around 42° is observed that is thought to stem from CoO, which is also majorly present at lower annealing temperatures (see ESI†). The effect of Mg doping in the lattice parameters was investigated *via* Rietveld method with GSAS-II[36] and according to the refinement results (see ESI† for further details), the purple $LiMg_{0.1}Co_{0.9}BO_3$ crystals have a monoclinic symmetry (space group: $C12/c1$) and a smaller unit cell (a = 5.1101(6) Å, b = 8.7962(8) Å, c = 10.0351(9) Å, β = 91.44(1)°, and V = 450.93(6) Å^3) compared to the unsubstituted $LiCoBO_3$ (a = 5.129(1) Å, b = 8.840(2) Å, c = 10.100(2) Å, β = 91.36(3)°, and V = 457.81(37) Å^3)[35] (Fig. 1d). The crystal structure of $LiMBO_3$ (M = Mg, Co) is shown in Fig. 1c. In the crystal system, Li atoms are coordinated by 4 O atoms and Co atoms are coordinated by 5 O atoms forming tetrahedra and trigonal-bipyramids, respectively. These two different polyhedra are connected to each other *via* corner and edge sharing and condensed to a polyhedral chain along [−1 0 1]. Two polyhedral chains are further interconnected through trigonal planar BO_3 units (Fig. 1c).

The substitution of Mg in the crystal lattice that was evidenced by the refinement results is further investigated by energy dispersive X-ray spectroscopy (EDX) analysis. The SEM-EDX micrographs indicate that Mg is homogenously distributed in $LiMg_{0.1}Co_{0.9}BO_3$ crystallites (Fig. 2 and ESI Fig. S2†). The elemental analysis within the limits of this technique shows that Mg/Co ratio is 0.09 per formula unit, which is close to the expected theoretical ratio of 0.11. SEM micrographs were used to investigate the morphology of $LiMg_{0.1}Co_{0.9}BO_3$ particles before and after the electrode preparation with reduced graphite oxide (rGO) and Super P carbon. The SEM micrographs in Fig. 3 show that the micron and submicron-sized crystallites of $LiMg_{0.1}Co_{0.9}BO_3$ form larger agglomerates, 15 μm to 50 μm in size. Relatively higher synthesis temperatures are considered to cause the larger agglomerates, as the gel-powder could only yield the phase pure active material when annealed at

Open Access Article. Published on 26 April 2018. Downloaded on 11/14/2018 9:13:47 AM.
This article is licensed under a Creative Commons Attribution-NonCommercial 3.0 Unported Licence.



(c)

Per Formula Unit	Mg	Co	O	Per Formula Unit	Mg / Co
EDX	0.07	0.81	3.16	EDX	0.09
Theoretical	0.10	0.90	3.00	Theoretical	0.11

Fig. 2 (a) Elemental map obtained by EDX (Mg and Co shown in green and red colours, respectively), (b) SEM micrograph of the mapped area, and (c) the atomic percentages of Mg, Co, and O obtained by EDX analysis and calculations according to the compound composition.

temperatures above 700–750 °C and other residual oxide impurities are found to exist when annealed at lower temperatures (ESI Fig. S3†). Nevertheless, these agglomerates could be ground to the submicron range particles that were completely coated with conductive carbon after mixing with rGO and carbon black forming a textured conducting composite electrode, see ESI Fig. S4.†

The electrochemical properties of $LiMg_{0.1}Co_{0.9}BO_3$ were investigated through galvanostatic cycling and cyclic voltammetry measurements. The cyclic voltammetry analysis for $LiMg_{0.1}Co_{0.9}BO_3$ was conducted at 0.05 mV s^{-1} rate between 4.7–1.7 V for four cycles (Fig. 4). The analysis shows broad oxidation and reduction processes indicating apparent polarisation in the system. The whole oxidation process extends from ~3.0 V till 4.7 V with a peak position at ~4.1 V that is in line with the previous findings based on plain $LiCoBO_3$.[23,26,29] A reduction peak can be observed at ~2.5 V and the whole process again spreads to a large potential window ~4.0–1.7 V.

The first five charge/discharge curves for $LiMg_{0.1}Co_{0.9}BO_3$ are displayed in Fig. 4a. The working electrode consisted of 70% active material, 10% conductive carbon, 10% reduced graphite oxide, and 10% PVDF with an active material loading of ~2 mg cm^{-2}. The measurement conducted within a 4.7–1.7 V voltage window at a rate of 10 mA g^{-1} and the active material delivers a first charge capacity of 36 mA h g^{-1} and a first discharge capacity of 32 mA h g^{-1}. The electrolyte chosen ($Li[(C_2F_5)_3PF_3]$ in EC : DMC (1 : 1), Merck, LF-30 SelectiLyte™) is expected to be stable at the chosen voltage window,[37] thus we do not expect any major contribution from the electrolyte oxidation or decomposition. The fifth discharge capacity is found to be 31.5 mA h g^{-1} indicating that the material is fairly stable upon cycling compared to the similar cathode systems.[16,24,29] The cycling properties of $LiMg_{0.1}Co_{0.9}BO_3$ within 4.7–1.7 V is presented in Fig. 4b for the first 10 cycles at a rate of 10 mA g^{-1} and at a rate of 20 mA g^{-1} for the next 10 subsequent cycles, respectively. The average discharge capacity drop at 10 mA g^{-1}

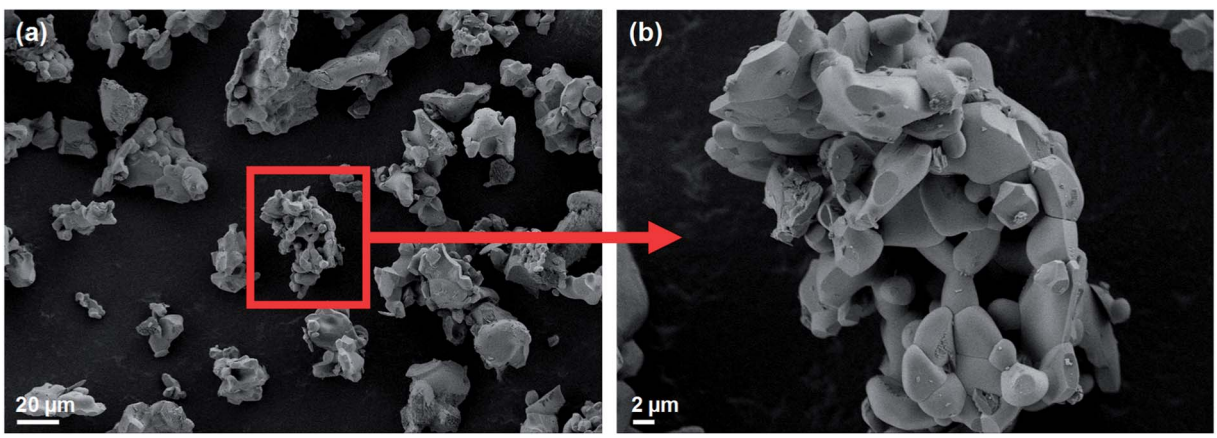


Fig. 3 SEM micrographs displaying (a) general view of $LiMg_{0.1}Co_{0.9}BO_3$ agglomerates and (b) magnified region in (a).

This journal is © The Royal Society of Chemistry 2018

Open Access Article. Published on 26 April 2018. Downloaded on 11/14/2018 9:13:47 AM.
This article is licensed under a Creative Commons Attribution-NonCommercial 3.0 Unported Licence.

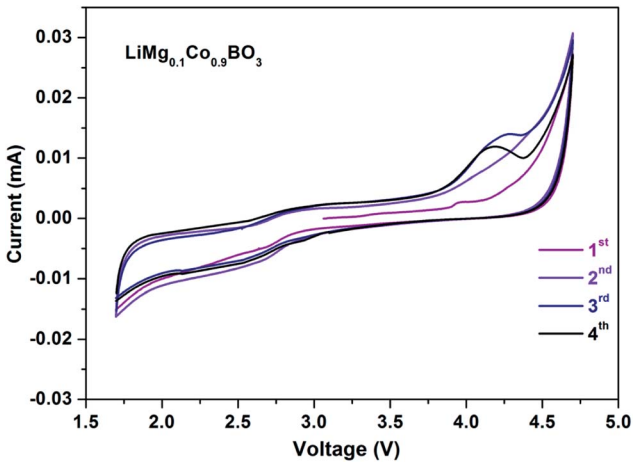


Fig. 4 Cyclic voltammogram (cycles #1–4) of rGO/C/$LiMg_{0.1}Co_{0.9}BO_3$ between 4.7–1.7 V recorded at 0.05 mV s^{-1} rate.

current rate is found to be ~1.3%, and a discharge capacity of ~25 mA h g^{-1} is still obtained at the 15th cycle when the current rate is increased to 20 mA g^{-1}. In order to evaluate the effects of Mg substitution on the electrochemical performance, unsubstituted micron-sized $LiCoBO_3$ (see ESI Fig. S5 and S6† for further details) was also obtained *via* sol–gel synthesis and tested under a similar protocol. To give a further edge for the Li^+ extraction in this kinetically limited system, a potentiostatic step at 4.7 V was applied till the current drops below 2 mA g^{-1}. The charge and discharge rates were kept same with the Mg substituted system at 10 mA g^{-1}. For the sol–gel synthesised micron-sized $LiCoBO_3$, a first charge capacity of ~17 mA h g^{-1} is obtained till the potentiostatic step, which reaches to ~27 mA h g^{-1} at the end of the potentiostatic step (Fig. 5c). The coulombic efficiency is lower than that of $LiMg_{0.1}Co_{0.9}BO_3$, as the capacity stays at ~21 mA h g^{-1} at the first discharge step (Fig. 5c). The cycling stability for the micron-sized $LiCoBO_3$ is also poorer compared to $LiMg_{0.1}Co_{0.9}BO_3$, as the discharge capacity drops to ~14 mA h g^{-1} at the 10th cycle with an average of loss ~3.25% at each cycle (Fig. 5d).

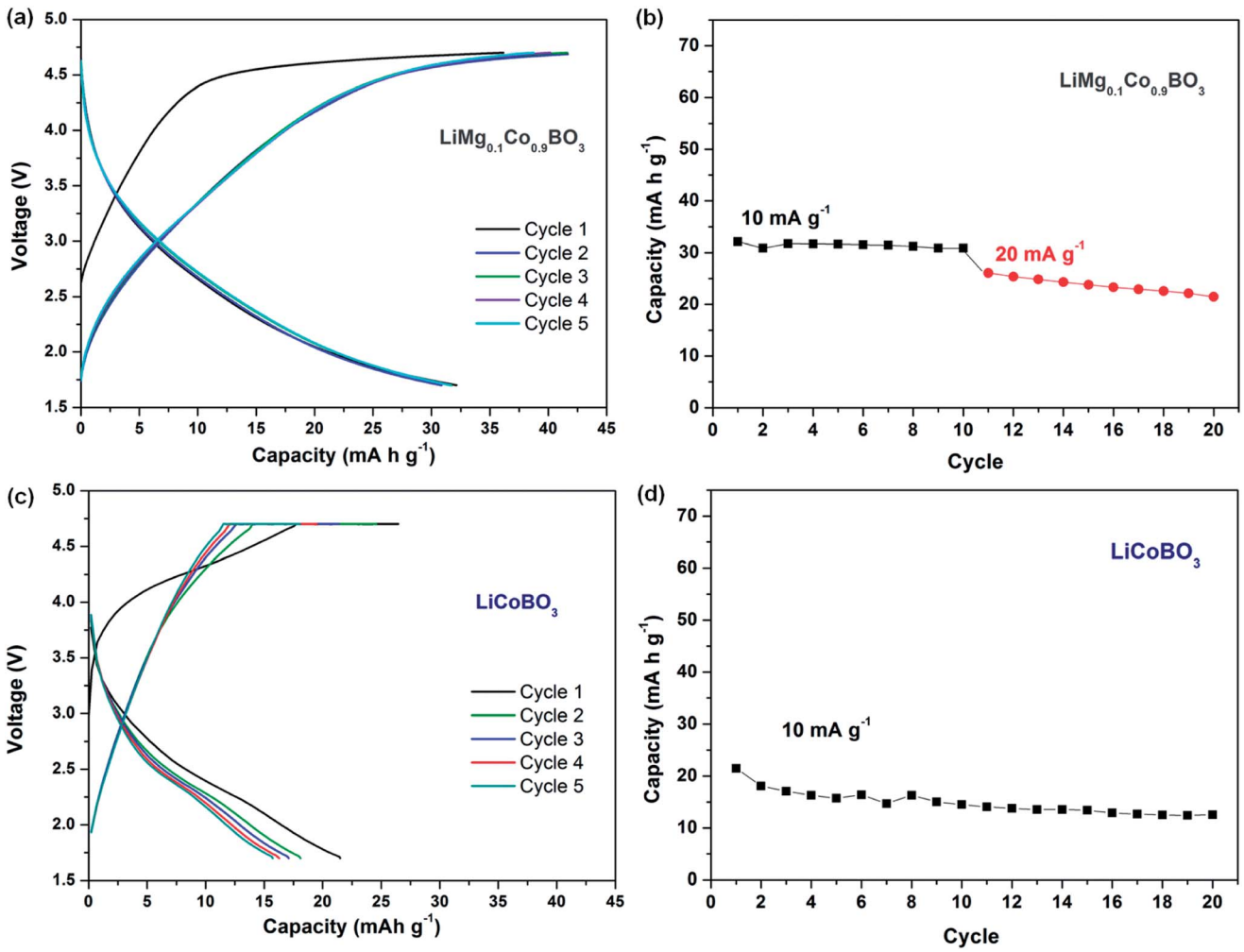


Fig. 5 (a) The first five charge/discharge curves of rGO/C/$LiMg_{0.1}Co_{0.9}BO_3$ recorded in a voltage window of 4.7–1.7 V with a rate of 10 mA g^{-1}, (b) the cycling stability of $LiMg_{0.1}Co_{0.9}BO_3$ for rates 10 mA g^{-1} and 20 mA g^{-1} within a 4.7–1.7 V voltage window, (c) the first five charge/discharge curves of rGO/C/$LiCoBO_3$ recorded in a voltage window of 4.7–1.7 V with a rate of 10 mA g^{-1} (constant voltage at 4.7 V until the current < 2 mA g^{-1}), and (d) the cycling stability of $LiCoBO_3$ at a rate of 10 mA g^{-1}.

Open Access Article. Published on 26 April 2018. Downloaded on 11/14/2018 9:13:47 AM. This article is licensed under a Creative Commons Attribution-NonCommercial 3.0 Unported Licence.

Though the electrochemical activity of $LiMg_{0.1}Co_{0.9}BO_3$ is shown here, the practical capacity obtained is still a fraction of the theoretical promise. The effect Mg substitution on the electrochemical performance of $LiCoBO_3$ is considered to be beneficial as a slight improvement in the capacity and cycling properties can be achieved (*e.g.* ~30 mA h g^{-1} for micron-sized $LiMg_{0.1}Co_{0.9}BO_3$ particles *vs.* ~1–6 mA h g^{-1} for micron-sized $LiCoBO_3$ particles[9,23]) compared to the similar size borate-based cathodes in the literature. Although the inertness of $LiCoBO_3$ as an electrode material was reported in some investigations,[27] we believe that the main reason for the poor electrochemical activity is the limited ionic and electronic conductivity in the system. The time for intercalation in nano-materials is 10^6 times less than micron-sized materials;[1] hence, the utilisation of nano-particles has been tried in various reports[12,16–18] with some success to overcome the conductivity issue as well as the kinetic polarisation problem. Here, we tried to apply both the substitution of the transition metal and the low dimensional composite electrode employment, however relatively large particles still exist in the electrode due to the processing method and draw the capacity of the synthesised material away from the theoretical capacity. Development of different conductive coatings and employment of nano-sized active material in the electrode fabrication could still improve the electrochemical performance of $LiMg_{0.1}Co_{0.9}BO_3$, as they do in previously reported polyanion cathodes.[1,12,23,25] Another approach could be the use of micron-sized active materials with mesopores rather than nano-sized materials[17] to overcome the disconnection problem between particles. Nevertheless, Mg substitution in $LiCoBO_3$ has been realised here through a sol–gel method and could be a viable way to further improve the electrochemical characteristics in the system when combined with other electrode enhancement techniques.

4. Conclusion

$LiMg_{0.1}Co_{0.9}BO_3$ was synthesised following a sol–gel method for the first time. The crystal structure and pertaining lattice parameters were investigated by X-ray powder diffraction and the homogenous distribution of Mg in the phase was confirmed by EDX analysis. An electrode mixture using the active material and conductive carbon (reduced graphite oxide and Super P carbon) was used in electrochemical tests including galvanostatic and cyclic voltammetry analyses. A first discharge capacity of 32 mA h g^{-1} was observed in galvanostatic cycling tests conducted within a 4.7–1.7 V voltage window at a rate of 10 mA g^{-1}. The realised electrochemical properties are relatively better compared to the similar sized $LiCoBO_3$. The obtained results suggest that Mg substitution may contribute positively towards the electrochemical properties of the material. Decreasing the particle size of the Mg substituted $LiCoBO_3$ and meticulous electrode engineering can further enhance the electrochemical performance of this system.

Conflicts of interest

There are no conflicts to declare.

Acknowledgements

The authors thank Koc University Surface Science and Technology Center (KUYTAM) for the use of characterisation facilities.

References

1 P. G. Bruce, *Solid State Ionics*, 2008, **179**, 752–760.
2 J. B. Goodenough and Y. Kim, *Chem. Mater.*, 2010, **22**, 587–603.
3 N. Nitta, F. X. Wu, J. T. Lee and G. Yushin, *Mater. Today*, 2015, **18**, 252–264.
4 M. Lee, J. Hong, D. H. Seo, D. H. Nam, K. T. Nam, K. Kang and C. B. Park, *Angew. Chem., Int. Ed.*, 2013, **52**, 8322–8328.
5 S. Y. Chung, J. T. Bloking and Y. M. Chiang, *Nat. Mater.*, 2002, **1**, 123–128.
6 J. Wolfenstine and J. Allen, *J. Power Sources*, 2004, **136**, 150–153.
7 G. H. Li, H. Azuma and M. Tohda, *Electrochem. Solid State*, 2002, **5**, A135–A137.
8 A. Manthiram and J. B. Goodenough, *J. Power Sources*, 1989, **26**, 403–408.
9 V. Legagneur, Y. An, A. Mosbah, R. Portal, A. L. La Salle, A. Verbaere, D. Guyomard and Y. Piffard, *Solid State Ionics*, 2001, **139**, 37–46.
10 A. Nyten, A. Abouimrane, M. Armand, T. Gustafsson and J. O. Thomas, *Electrochem. Commun.*, 2005, **7**, 156–160.
11 J. C. Kim, D. H. Seo and G. Ceder, *Energy Environ. Sci.*, 2015, **8**, 1790–1798.
12 H. Huang, S. C. Yin, T. Kerr, N. Taylor and L. F. Nazar, *Adv. Mater.*, 2002, **14**, 1525–1528.
13 Y. B. Lin, Y. Lin, T. Zhou, G. Y. Zhao, Y. D. Huang and Z. G. Huang, *J. Power Sources*, 2013, **226**, 20–26.
14 Y. S. Hu, Y. G. Guo, R. Dominko, M. Gaberscek, J. Jamnik and J. Maier, *Adv. Mater.*, 2007, **19**, 1963–1966.
15 Y. H. Huang, K. S. Park and J. B. Goodenough, *J. Electrochem. Soc.*, 2006, **153**, A2282–A2286.
16 S. Afyon, D. Kundu, F. Krumeich and R. Nesper, *J. Power Sources*, 2013, **224**, 145–151.
17 F. Jiao, K. M. Shaju and P. G. Bruce, *Angew. Chem., Int. Ed.*, 2005, **44**, 6550–6553.
18 S. L. Yang, X. F. Zhou, J. G. Zhang and Z. P. Liu, *J. Mater. Chem.*, 2010, **20**, 8086–8091.
19 M. Moradi, J. C. Kim, J. F. Qi, K. Xu, X. Li, G. Ceder and A. M. Belcher, *Green Chem.*, 2016, **18**, 2619–2624.
20 Y. S. Lee and H. Lee, *Electron. Mater. Lett.*, 2014, **10**, 253–258.
21 A. Yamada, N. Iwane, Y. Harada, S. Nishimura, Y. Koyama and I. Tanaka, *Adv. Mater.*, 2010, **22**, 3583–3587.
22 Y. Yamashita, P. Barpanda, Y. Yamada and A. Yamada, *ECS Electrochem. Lett.*, 2013, **2**, A75–A77.
23 S. Afyon, C. Mensing, F. Krumeich and R. Nesper, *Solid State Ionics*, 2014, **256**, 103–108.
24 A. P. Tang, Q. W. Zhong, G. R. Xu and H. S. Song, *RSC Adv.*, 2016, **6**, 84439–84444.
25 V. Ragupathi, S. Krishnaswamy, S. Raman, P. Panigrahi, J. Lee and G. S. Nagarajan, *Appl. Surf. Sci.*, 2017, DOI: 10.1016/j.apsusc.2017.11.087.

 This journal is © The Royal Society of Chemistry 2018

Open Access Article. Published on 26 April 2018. Downloaded on 11/14/2018 9:13:47 AM.
This article is licensed under a Creative Commons Attribution-NonCommercial 3.0 Unported Licence.



26 O. A. Drozhzhin, I. V. Tereshchenko and E. V. Antipov, *Ceram. Int.*, 2017, **43**, 4670–4673.
27 S. H. Bo, G. M. Veith, M. R. Saccomanno, H. F. Huang, P. V. Burmistrova, A. C. Malingowski, R. L. Sacci, K. R. Kittilstved, C. P. Grey and P. G. Khalifah, *ACS Appl. Mater. Interfaces*, 2014, **6**, 10840–10848.
28 B. Le Roux, C. Bourbon, O. I. Lebedev, J. F. Colin and V. Pralong, *Inorg. Chem.*, 2015, **54**, 5273–5279.
29 B. Le Roux, C. Bourbon, J. F. Colin and V. Pralong, *RSC Adv.*, 2015, **5**, 72801–72804.
30 J. C. Kim, X. Li, C. J. Moore, S. H. Bo, P. G. Khalifah, C. P. Grey and G. Ceder, *Chem. Mater.*, 2014, **26**, 4200–4206.
31 L. Qu, D. Luo, S. H. Fang, Y. Liu, L. Yang, S. Hirano and C. C. Yang, *J. Power Sources*, 2016, **307**, 69–76.
32 M. V. Reddy, T. W. Jie, C. J. Jafta, K. I. Ozoemena, M. K. Mathe, A. S. Nair, S. S. Peng, M. S. Idris, G. Balakrishna, F. I. Ezema and B. V. R. Chowdari, *Electrochim. Acta*, 2014, **128**, 192–197.
33 J. H. Shim, J. Lee, S. Y. Han and S. Lee, *Electrochim. Acta*, 2015, **186**, 201–208.
34 S. Levasseur, M. Menetrier and C. Delmas, *Chem. Mater.*, 2002, **14**, 3584–3590.
35 Y. Piffard, K. K. Rangan, Y. L. An, D. Guyomard and M. Tournoux, *Acta Crystallogr., Sect. C: Cryst. Struct. Commun.*, 1998, **54**, 1561–1563.
36 B. H. Toby and R. B. Von Dreele, *J. Appl. Crystallogr.*, 2013, **46**, 544–549.
37 M. Schmidt, U. Heider, A. Kuehner, R. Oesten, M. Jungnitz, N. Ignat'ev and P. Sartori, *J. Power Sources*, 2001, **97–8**, 557–560.